Supplement of

Viscosity and phase state of aerosol particles consisting of sucrose mixed with inorganic salts

Young-Chul Song et al.,

Correspondence to: Mijung Song (mijung.song@jbnu.ac.kr)

• SI_LLPS_Song_submitted.docx

S1. Measurements of bead speeds of particles

Renbaum-Wolff et al. (2013a) introduced the method of the bead-mobility technique to determine viscosity of aerosol particles. In this study, bead speeds were measured at different relative humidity (RH) and then the bead speeds were converted to viscosities using a calibration line (Fig. S1). The calibration line was produced by measurement of bead speeds as a function of viscosities of sucrose/H_2O particles at different RH. The values were fit to a power function, *bead speeds (μm/ms) = a ×* (viscosity *(Pa s)*, *η*) ^{b}. *a*, *b* are the best-fit parameters, and used $a = 1.84 \times 10^{-4}$ and $b = -1.08$ in this study. The values agree well with the previous study of Renbaum-Wolff et al. (2013a).
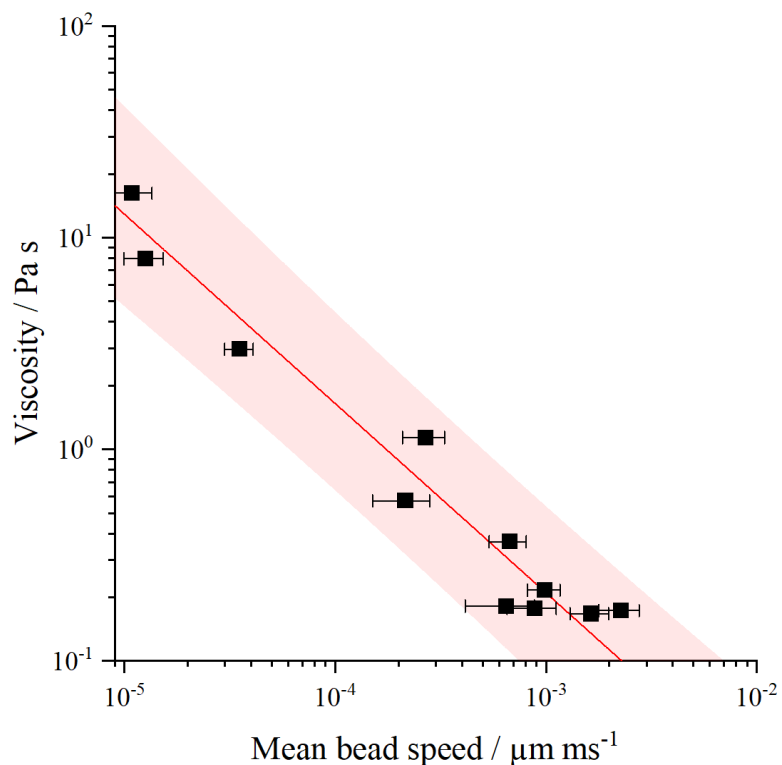
20 Figure S1. A calibration line of mean bead speeds as a function of viscosities of sucrose/H_2O particles at
different RH. The red line indicates a best-fit line and pink envelopes indicate the 95% prediction bands
of the fitting in sucrose/H_2O particles. The mean bead speed error bars (on x-axis) represent the standard
deviation from the measurements of 3-5 beads per particle at a given relative humidity.

25   Figure S2 shows the mean bead speeds at different RH of sucrose/H_2O (Fig. S2a), $Mg(NO_3)_2$/H_2O and $Ca(NO_3)_2$/H_2O (Fig. S2b), and sucrose/$Mg(NO_3)_2$/H_2O and sucrose/$Ca(NO_3)_2$/H_2O (Fig. S2c). The bead speeds of the sucrose/H_2O particles decreased from $\sim 9 \times 10^{-4}$ to $\sim 1 \times 10^{-5}$ $\mu m \cdot ms^{-1}$ when the RH decreased from ~ 85 to ~ 69 % RH (Fig. S2a). In Fig. S2b, the mean bead speeds of $Mg(NO_3)_2$/H_2O decreased from $\sim 5 \times 10^{-2}$ to 6×10^{-3} $\mu m \cdot ms^{-1}$ as the RH reduced from ~ 66 to $\sim 35\%$, and the speeds of $Ca(NO_3)_2$/H_2O

30   decreased from 9×10^{-3} to 1×10^{-6} $\mu m \cdot ms^{-1}$ as the RH decreased from ~ 62 to $\sim 12\%$. The mean bead speeds of sucrose/$Mg(NO_3)_2$/H_2O particles decreased from $\sim 6 \times 10^{-3}$ to $\sim 1 \times 10^{-5}$ $\mu m \cdot ms^{-1}$ at RH ranges from ~ 68 to $\sim 35\%$, and the bead speeds of the sucrose/$Ca(NO_3)_2$/H_2O particles reduced from $\sim 8 \times 10^{-3}$ to $\sim 5 \times 10^{-6}$ $\mu m \cdot ms^{-1}$ as the RH decreased from ~ 80 to $\sim 40\%$ RH (Fig. S2c). These bead speeds of the particles were converted to the viscosities using the calibration line shown in Fig. S1.
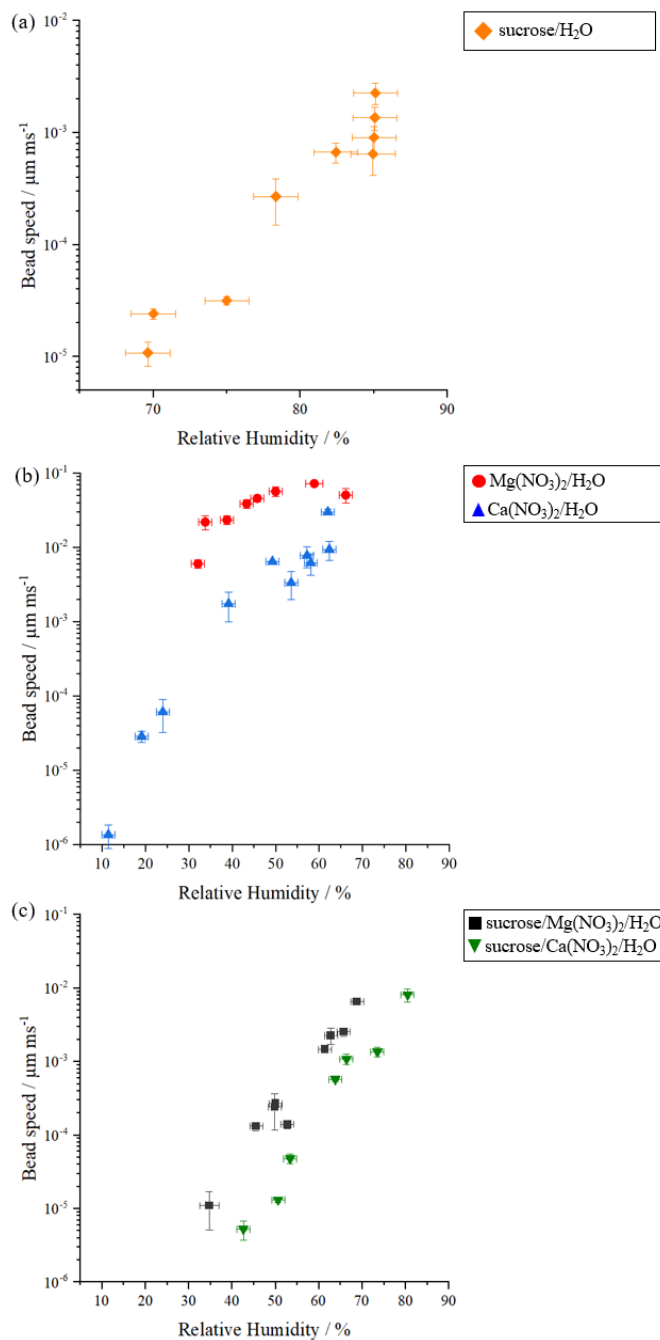
Figure S2. The bead speeds of each species as function of relative humidity (RH). (a) sucrose/H_2O, (b) $Mg(NO_3)_2$/H_2O and $Ca(NO_3)_2$/H_2O, and (c) sucrose/$Mg(NO_3)_2$/H_2O and sucrose/$Ca(NO_3)_2$/H_2O particles. The *x* error bars indicate the uncertainty in the RH measurements. The mean bead speed error bars (on y-axis) represent the standard deviation from the measurements of 3-5 beads per particle at a given RH.

S2. Poke-and-flow experiments

Figure S3 illustrates the optical images of sucrose/H_2O, sucrose/$Ca(NO_3)_2$/H_2O, and sucrose/$Mg(NO_3)_2$/H_2O particles from pre-poking, poking, and post-poking. Using the ImageJ software, the area of the inner hole was calculated and the experimental flow time was determined when the area decreased to 1/4 of the initial area. Figure S3 shows the experimental flow time of the sucrose/H_2O particles at 43% RH as 207 s, sucrose/$Ca(NO_3)_2$/H_2O particles at 30% RH as 39 s, and sucrose/$Mg(NO_3)_2$/H_2O particles at 17% RH as 73 s. After the determining the experimental flow time ($\tau_{(exp, flow)}$) of the particles, the equation from Sellier et al. (2015) was applied to calculate viscosity. The $\tau_{(exp, flow)}$ of the particles was converted to the lower limit to viscosity using the equation, *The experimental timescale (s) = 0.0032×(Viscosity (Pa s))+2.1×10^{-7}*. For example, Fig. S3a shows an example of the optical images of sucrose/H_2O at 43% RH. The $\tau_{(exp, flow)}$ of this particle was 207 s, so that the lower limit to the dynamic viscosity was calculated as $\sim6\times10^4$ Pa s. In this study, the upper limit to viscosity is unknown from the poke-and-flow technique. Figure S4a-c shows the $\tau_{(exp, flow)}$ of sucrose/H_2O, sucrose/$Ca(NO_3)_2$/H_2O, and sucrose/$Mg(NO_3)_2$/H_2O particles as function of RH.

In this work, the viscosities at RH where particles cracked were determined using the poke-and-flow technique (Renbaum-Wolff et al., 2013b; Grayson et al., 2015), based on the viscosity-value where secondary organic aerosol particles cracked from previous studies (Renbaum-Wolff et al., 2013b; Grayson et al., 2015; Song et al., 2016, 2019). Previous studies obtained the lower limit of the viscosities using a fluid simulation with the lower limit of physical parameters (density, contact angle, slip length, and surface tension) and a fixed geometry with a quarter-sphere diameter (20 μm) which is similar what was observed in the poke-and-flow experiment after particles cracked (Renbaum-Wolff et al., 2013b; Song et al., 2016, 2019). In this study, the lower limit of contact angles for the sucrose, $Ca(NO_3)_2$ and $Mg(NO_3)_2$ were measured as ~72 °, ~93 °, ~93 ° for ~5 μl of each droplet deposited on a hydrophobic substrate. The lower limit of surface tension of sucrose, $Ca(NO_3)_2$, $Mg(NO_3)_2$ are from the literature (Dutcher et al., 2010; Lee and Hildemann, 2013; Grayson et al., 2015). The lower limit of density was assumed to be the density of pure water. The lower limit of slip length was assumed to be 5 nm as described in previous work (Churaev et al., 1984; Baudry et al., 2001; Joseph and Tabeling, 2005; Renbaum-Wolff et al., 2013b; Li et al., 2014; Grayson et al., 2015). These lower limits of the contact

angle, surface tension, density, and slip length are included as the lower limits of the physical parameters that were used in previous studies employing the poke-and-flow technique (Renbaum-Wolff et al., 2013b; Graysong et al., 2015; Song et al., 2016, 2019). Thus, we defined the lower limit of the viscosities as ~10^8 Pa s when a particle cracked during poke-and-flow experiments.
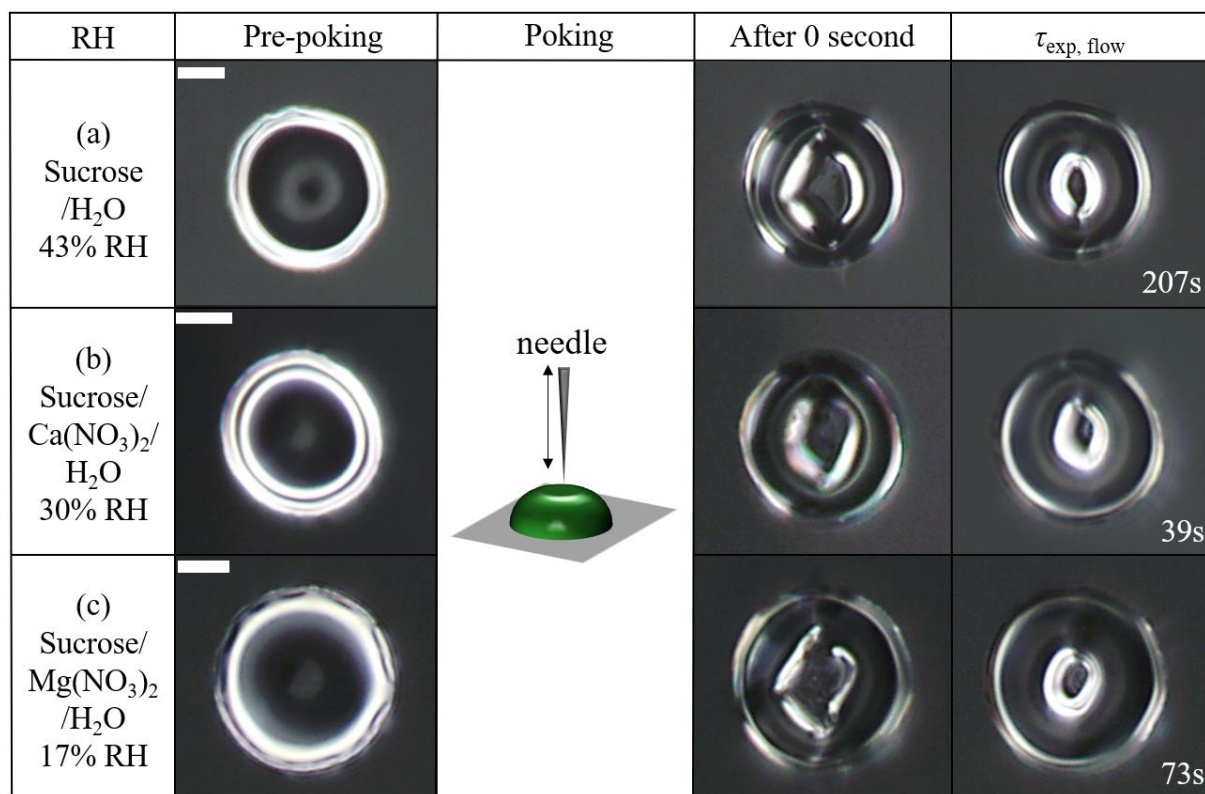
Figure S3. Optical images during poke-and-flow experiments at the points of pre-poking, poking, and post-poking for particles consisting of (a) sucrose/H_2O, (b) sucrose/Ca(NO$_3$)$_2$/H_2O, and (c) sucrose/Mg(NO$_3$)$_2$/H_2O particles. The scale bar is 10 µm.
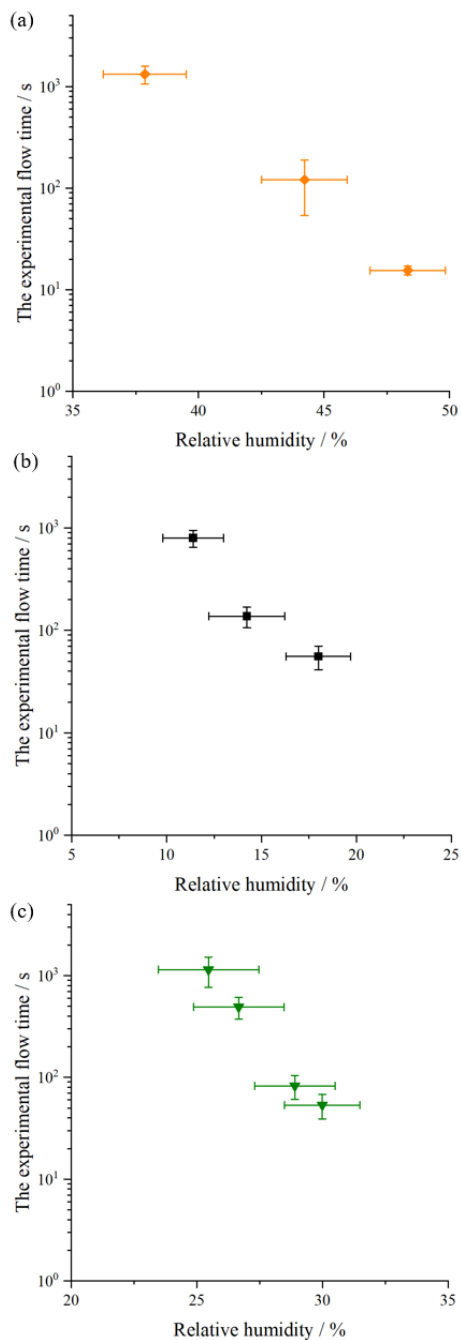
Figure S4. The experimental flow time of each species as function of relative humidity (RH) from poke-and-flow experiments. (a) sucrose/H_2O, (b) sucrose/$Mg(NO_3)_2$/H_2O, and (c) sucrose/$Ca(NO_3)_2$/H_2O particles. The *x* error bars indicate the uncertainty in the RH measurements. The *y* error bars indicate a standardization of 3 - 4 of poke-and-flow experiments at a given RH.

S3. The morphologies of the particles during dehydrate cycles

We investigated the optical morphologies of the particles upon drying from ~100 to 0 % RH using an optical microscope (Olympus BX43 with 40× objective). Figure S5 presents the optical images of sucrose/H_2O, Mg(NO$_3$)$_2$/H_2O, Ca(NO$_3$)$_2$/H_2O, sucrose/Ca(NO$_3$)$_2$/H_2O, and sucrose/Mg(NO$_3$)$_2$/H_2O particles during dehydration and hydrate cycles.
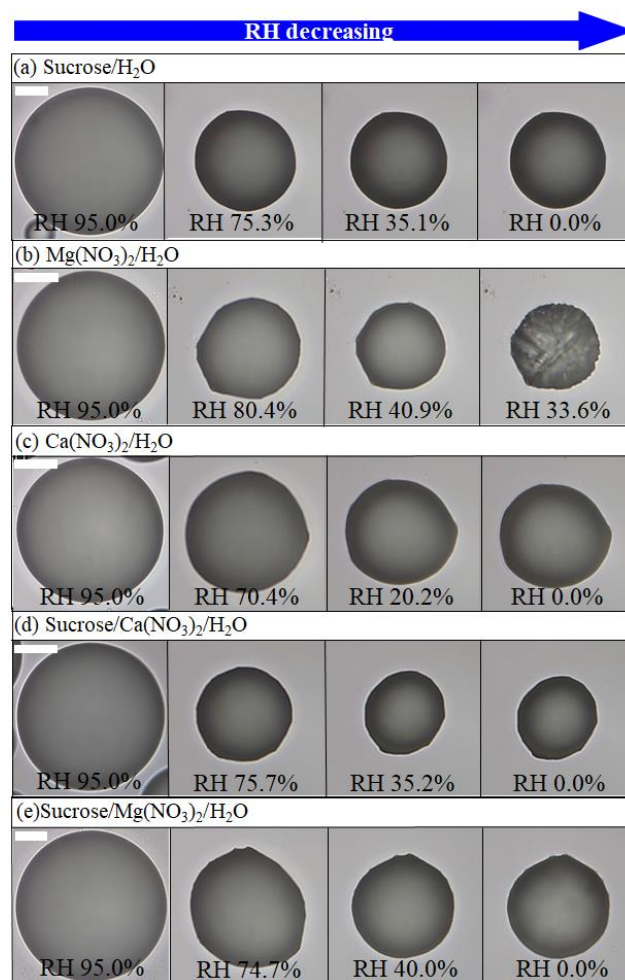
Figure S5. Optical images of (a) sucrose/H_2O, (b) Mg(NO$_3$)$_2$/H_2O, (c) Ca(NO$_3$)$_2$/H_2O, (d) sucrose/Ca(NO$_3$)$_2$/H_2O, (e) sucrose/Mg(NO$_3$)$_2$/H_2O particles on drying with a rate of 0.3% - 0.5% RH min^{-1}. The white scale bar indicates 20 μm.

S4. Parameterization of viscosities

Parametrization of the RH as a function of the viscosities of the particles investigated was obtained using a 2nd order polynomial fit in log-scale (Fig. 4). Table S1 provides the parameterization of viscosities of each system.

Table S1. Parametrization of viscosities of different particles. η denotes viscosity (unit: Pa s).

System	Parameterization	Relative humidity (RH) range
sucrose/H_2O	$\log_{10}(\eta) = 11.9 - 0.16 \times RH + 1.2 \times 10^{-4} \times RH^2$	24% < RH < 100%
$Ca(NO_3)_2$/H_2O	$\log_{10}(Viscosity\ (\eta)) = 2.5 - 0.10 \times RH + 4.2 \times 10^{-4} \times RH^2$	6% < RH < 100%
$Mg(NO_3)_2$/H_2O	$\log_{10}(Viscosity\ (\eta)) = -1.4 - 0.02 \times RH + 1.8 \times 10^{-5} \times RH^2$	31% < RH < 100%
sucrose/$Ca(NO_3)_2$/H_2O	$\log_{10}(Viscosity\ (\eta)) = 10.4 - 0.23 \times RH + 9.9 \times 10^{-4} \times RH^2$	13% < RH < 100%
sucrose/$Mg(NO_3)_2$/H_2O	$\log_{10}(Viscosity\ (\eta)) = 9.0 - 0.23 \times RH + 1.1 \times 10^{-3} \times RH^2$	6% < RH < 100%

S5. AIOMFAC-VISC with ZSR mixing rule for aqueous organic–salt systems

The deployed mixing effects of organic and inorganic solutes on phase viscosity need to be considered with the AIOMFAC-VISC model. Different possible mixing models may be introduced. The approach deployed in this work is a ZSR-type mixing rule (see main text Sect. 2.4), which is briefly characterized in the following. The goal of our method is to split the system conceptually into a salt-free aqueous organic subsystem (subsystem 1) and an organic-free aqueous electrolyte subsystem (subsystem 2), such that we can compute the individual mixture viscosities (η_1, η_2) of those subsystems with AIOMFAC-VISC at the same water activity (RH) as is computed by AIOMFAC for the whole mixed organic–inorganic system. The mixture viscosity of the full (ternary) system is then estimated using a weighted arithmetic mean of the logarithms of subsystem viscosities; formally,

$$\ln(\eta/\eta°) = f_1 \ln(\eta_1/\eta°) + f_2 \ln(\eta_2/\eta°), \tag{S1}$$

where f_1, f_2 are weighting factors for the relative mass contributions from the subsystems, as described in the following, and $\eta°$ denotes unit viscosity (1 Pa s).

115 In the ternary case, we can use mass conservation and describe the total mass of the system (m) as

$$m = m_{org} + m_{el} + m_w, \tag{S2}$$

where subscripts org, el, and w denote, the organic, electrolyte (salt) and water components, respectively. Similarly, we can define the masses of the two subsystems, e.g. for the aqueous organic subsystem, $m_1 = m_{org,1} + m_{w,1}$, with subscript 1 denoting the subsystem and analogously for subsystem 2. Using a ZSR-

120 type mixing rule, at any given water activity, the ternary system can be approximated as an additive combination of the two subsystems in terms of water content and organic and inorganic contributions. Here we define $m_{org} = m_{org,1}$ and $m_{el} = m_{el,2}$, such that we can express the organic-to-inorganic dry mass ratio (OIR) as

$$\text{OIR} = \frac{m_{org}}{m_{el}} = \frac{m_{org,1}}{m_{el,2}} = \frac{w_{org,1}}{w_{el,2}} \frac{m_1}{m_2}. \tag{S3}$$

125 Here, $w_{org,1}$ is the mass fraction of the organic (sucrose) in subsystem 1 (relative to that subsystem's composition) and $w_{el,2}$ the mass fraction of the electrolyte (salt) in subsystem 2. We define the fractional contributions of masses from the two subsystems to the approximated mass of the whole system as $f_1 = \frac{m_1}{m_1+m_2}$, hence $f_2 = 1 - f_1$. Based on these definitions, it follows that

$$f_1 = \frac{\text{OIR} \times w_{el,2}}{w_{org,1} + \text{OIR} \times w_{el,2}}. \tag{S4}$$

130 Using these weighting factors in Eq. (S1) allows for a predictive estimation of the mixture viscosity while ensuring that the target OIR is met. The mass fractions $w_{org,1}$ and $w_{el,2}$ result from the composition prediction at given water activity (equil. RH), here using the AIOMFAC model. Therefore, note that the values of the weights f_1, f_2, are not constant for a constant OIR; rather they must be computed at each water activity level.

135

References

Baudry, J., Charlaix, E., Tonck, A., and Mazuyer, D.: Experimental evidence for a large slip effect at a nonwetting fluid-solid interface, Langmuir, 17, 5232–5236, doi:10.1021/La0009994, 2001.

Churaev, N. V., Sobolev, V. D., and Somov, A. N.: Slippage of liquids over lyophobic solid-surfaces, J. Colloid Interf. Sci., 97, 574–581, doi:10.1016/0021-9797(84)90330-8, 1984.

Dutcher, C. S., Wexler, A. S. and Clegg, S. L.: Surface tensions of inorganic multicomponent aqueous electrolyte solutions and melts, J. Phys. Chem. A, 114(46), 12216–12230, doi:10.1021/jp105191z, 2010.

Grayson, J. W., Song, M., Sellier, M. and Bertram, A. K.: Validation of the poke-flow technique combined with simulations of fluid flow for determining viscosities in samples with small volumes and high viscosities, Atmos. Meas. Tech., 8(6), 2463–2472, doi:10.5194/amt-8-2463-2015, 2015.

Joseph, P. and Tabeling, P.: Direct measurement of the apparent slip length, Phys. Rev. E., 71, 035303, doi:10.1103/Physreve.71.035303, 2005.

Li, L., Mo, J. W., and Li, Z. L.: Flow and slip transition in nanochannels, Phys. Rev. E., 90, 033003, doi:10.1103/Physreve.90.033003, 2014.

Lee, J. Y. and Hildemann, L. M.: Surface tension of solutions containing dicarboxylic acids with ammonium sulfate, d-glucose, or humic acid, J. Aerosol Sci., 64, 94–102, doi:10.1016/j.jaerosci.2013.06.004, 2013.

Renbaum-Wolff, L., Grayson, J. W. and Bertram, A. K.: Technical Note: New methodology for measuring viscosities in small volumes characteristic of environmental chamber particle samples, Atmos. Chem. Phys., 13(2), 791–802, doi:10.5194/acp-13-791-2013, 2013a.

Renbaum-Wolff, L., Grayson, J. W., Bateman, A. P., Kuwata, M., Sellier, M., Murray, B. J., Shilling, J. E., Martin, S. T. and Bertram, A. K.: Viscosity of a-pinene secondary organic material and implications for particle growth and reactivity, Proc. Natl. Acad. Sci., 110(20), 8014–8019, doi:10.1073/pnas.1219548110, 2013b.

Sellier, M., Grayson, J. W., Renbaum-Wolff, L., Song, M. and Bertram, A. K.: Estimating the viscosity of a highly viscous liquid droplet through the relaxation time of a dry spot, J. Rheol., 59(3), 733–750, doi:10.1122/1.4917240, 2015.

Song, M., Liu, P. F., Hanna, S. J., Zaveri, R. A., Potter, K., You, Y., Martin, S. T. and Bertram, A. K.: Relative humidity-dependent viscosity of secondary organic material from toluene photo-oxidation and possible implications for organic particulate matter over megacities, Atmos. Chem. Phys., 16(14), 8817–8830, doi:10.5194/acp-16-8817-2016, 2016.

170 Song, M., Maclean, A. M., Huang, Y., Smith, N. R., Blair, S. L., Laskin, J., Laskin, A., DeRieux, W.-S. W., Li, Y., Shiraiwa, M., Nizkorodov, S. A. and Bertram, A. K.: Liquid-liquid phase separation and viscosity within secondary organic aerosol generated from diesel fuel vapors, Atmos. Chem. Phys., 19(19), 12515–12529, doi:10.5194/acp-2019-367, 2019.